Flow and heat transfer characteristics of a novel airfoil-based tube with dimples

Houju PEI [1] *, Meinan LIU [2], Kaijie YANG [3], Zhimao LI [1], and Chao LIU [1]

[1] Shanghai Aircraft Design and Research Institute Environment Control and Oxygen System Department, China
[2] College of Energy and Power Engineering, Jiangsu University of Science and Technology, China
[3] Key Laboratory of Aircraft Environment Control and Life Support, MIIT, Nanjing University of Aeronautics and Astronautics, China

Abstract. The performance of a novel airfoil-based tube with dimples is numerically studied in the present work. The effect of Reynolds number Re, dimples number N, relative depth H/D, and cross-distribution angle α on flow and heat transfer characteristics are discussed for Re in the range between 7,753 and 21,736. The velocity contour, temperature contour, and local streamlines are also presented to get an insight into the heat transfer enhancement mechanisms. The results show that both the velocity magnitude and flow direction change, and fluid dynamic vortexes are generated around the dimples, which intensify the flow mixing and interrupt the boundary layer, resulting in a better heat transfer performance accompanied by a certain pressure loss compared with the plain tube. The Nusselt number Nu of the airfoil-based tube increases with the increase of dimples number, relative depth, and Reynolds numbers, but the effect of cross-distribution angle can be ignored. Under geometric parameters considered, the airfoil-based tube with $N = 6$, $H/D = 0.1$, $\alpha = 0°$ and Re $= 7,753$ can obtain the largest average PEC value 1.23. Further, the empirical formulas for Nusselt number Nu and friction factor f are fitted in terms of dimple number N, relative depth H/D, and Reynolds number Re, respectively, with the errors within $\pm 5\%$. It is found that the airfoil-based tube with dimples has a good comprehensive performance.

Key words: heat transfer enhancement; airfoil-based tube; dimple; comprehensive performance.

1. INTRODUCTION

Enhancing the efficiency of heat transfer plays a key role in solving energy issues [1]. Generally, heat transfer enhancement techniques can be grouped into active and passive techniques. As a typical passive heat transfer enhancement technology, dimples have been extensively used because of their obvious advantages with respect to simple structure, excellent capacities of heat transfer, and relatively low-pressure loss penalty [2–7]. The majority of previous studies on dimples have largely focused on rectangular or cylindrical channels, as shown in Fig. 1. The arrangement is usually a conventional tube with concave or convex spherical dimples on the surface of the channel.

The heat transfer and flow characteristics have been numerically investigated in the cross-combined dimple tube (Fig. 1a) by Zhang *et al.* [8]. Wang *et al.* [9] and Liao *et al.* [10] studied the effect of a spherical dimpled tube (Fig. 1b) and ellipsoidal dimpled tube (Fig. 1c), respectively, on heat transfer and flow characteristics. Zhang *et al.* [11] studied the flow and heat transfer performance of a new type of biomimetic tube (Fig. 1d). Xie *et al.* [12] numerically investigated the heat transfer enhancement mechanisms of an enhanced tube with cross ellipsoidal dimples (Fig. 1e). It is found that the transverse and longitudinal dimples can cause downward flow, improve the flow mixing and reattachment, interrupt the boundary layer, and then greatly improve the heat transfer performance. Shi *et al.* [13] proposed a novel airfoil PCHE with dimples (Fig. 1f). In the range of Reynolds number studied, the comprehensive performance can be improved by 3.5%~8.7%. Li *et al.* [14] reported that when the Reynolds number is low, the heat transfer efficiency of a tube with smaller dimples is higher, which is opposite to that with a high Reynolds number. Chen *et al.* [15] compared four NACA 00XX series fin PCHEs (printed circuit heat exchangers) to investigate the influence of airfoil profile on flow and heat transfer performance. Among the four NACA airfoil fin PCHEs, NACA 0010 airfoil fin PCHE demonstrates the best comprehensible performance.

Previous works mainly pay attention to enhanced tubes with rectangular or cylindrical channels. However, rare investigations have been reported for the newly designed airfoil-based tube. The object of this study is to provide a prediction of its flow and heat transfer characteristics in the range of the Reynolds number from 7,753 to 21,736. The effect of the Reynolds number, dimples number, relative depth, and cross-distribution angle on performance are discussed. Also, the mechanisms of heat transfer enhancement are analyzed by the velocity contour, temperature contour, and local streamlines.

*e-mail: hj_pei@nuaa.edu.cn

(a) cross-combined ellipsoidal dimple tube [8]

(b) spherical dimpled tube [9]

(c) ellipsoidal dimpled tube [10]

(d) biomimetic tube [11]

(e) cross ellipsoidal dimple [12]
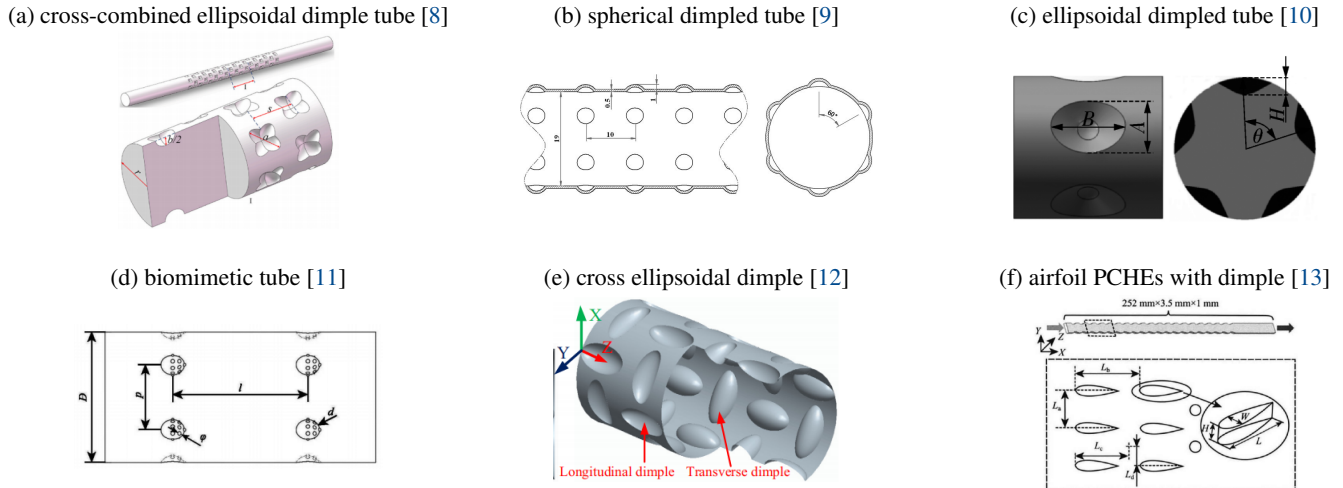
(f) airfoil PCHEs with dimple [13]

Fig. 1. Schematic of different types of dimpled tube

2. GEOMETRY MODEL

Figure 2 shows the geometric schematic of the airfoil-based tube with dimples used in the present study. The length L is 100 mm, the diameter D is 20 mm. NACA0012 standard airfoil (Fig. 2b) is adopted with an airfoil length of 20 mm and an aspect ratio of 50/3. In consideration of the full-developed flow and backflow at the outlet boundary, the extended section with a length of $4.5L$ is defined both upstream and downstream (Fig. 2a). The drawing of the airfoils and dimples section is shown in Fig. 2c. The main geometric parameters include dimple number N, relative depth H/D (where H is the depth of the dimple, as shown in Fig. 2d, D is the diameter of the airfoil-based tube), and cross-distribution angle α. The primary geometric parameters are $N = 3$, $H/D = 0.1$ ($H = 2$ mm) and $\alpha = 0°$. The arrangement for different cases is listed in Table 1.
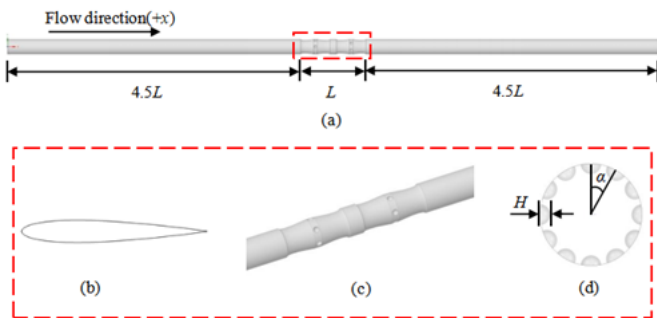
Fig. 2. Geometry model of the airfoil-based tube: (a) NACA0012 airfoil; (b) airfoil and dimple section; (c) cross distribution angle and relative depth of the dimple

Table 1
Values of the geometric parameters

N	H/D	α [°]
3, 4, 5, 6	0.1	0
6	0.1, 0.075, 0.05, 0.025	0
3, 4, 5, 6	0.1	0, 10, 20, 30

3. NUMERICAL METHOD

3.1. Governing equation

In the present work, continuity equation, momentum equation, and energy equation are used to describe the flow and heat transfer characteristics.

Continuity equation:

$$\nabla \cdot (\rho \vec{u}) = 0. \tag{1}$$

Momentum equation:

$$\nabla \vec{u} \cdot (\rho \vec{u}) = -\nabla P - \frac{2}{3}\nabla[\mu(\nabla \cdot \vec{u})] + \nabla \cdot \left[\mu(\nabla \vec{u})^T\right] + \nabla \cdot [\mu(\nabla \vec{u})]. \tag{2}$$

Energy equation:

$$\rho C_p \vec{u} \cdot \nabla T = \nabla[\lambda(\nabla T)] + \vec{u} \cdot \nabla P + \varphi, \tag{3}$$

where ρ, P, T, μ, λ and C_p represent density, pressure, temperature, viscosity coefficient, heat transfer coefficient, and specific heat at a constant pressure of the flowing medium, respectively. φ is the viscous dissipation and $\vec{u}$ is the velocity vector.

In consideration of its accuracy, the realizable k-ε turbulence model and enhanced wall function are used in the study of flow and heat transfer characteristics of an enhanced tube [16, 17] and the simulation results will also be validated.

3.2. Non-dimensional parameters

Several non-dimensional parameters used in the present work are expressed as follows:

Reynolds number (Re):

$$\text{Re} = \rho V D / \mu. \tag{4}$$

Nusselt number (Nu):

$$\text{Nu} = hD/\lambda. \tag{5}$$

2

Bull. Pol. Acad. Sci. Tech. Sci., vol. 70, no. 4, p. e141984, 2022

Prandtl number (Pr):

$$Pr = C p \mu / \lambda. \tag{6}$$

Friction factor (f) [12]:

$$f = 2 \Delta p D / \rho V^2 L, \tag{7}$$

where Δp is the pressure drop of the tube, V is the fluid velocity.

Comprehensive performance evaluation criteria (PEC) [18–20]:

$$PEC = \frac{Nu/Nu_0}{(f/f_0)^{1/6}}, \tag{8}$$

where Nu_0 and f_0 are the Nusselt number and friction factor of the plain tube, respectively.

3.3. Grid details, boundaries, and grid independence validation

3.3.1. Grid details

In the numerical simulation, the unstructured hybrid grids are generated, as shown in Fig. 3. In addition, the prism grids near the tube wall (Fig. 3b) are refined enough (the first grid height is set to 3.5×10^{-5} m) to ensure that the wall $y+ \approx 1$.

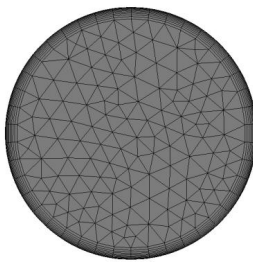(a) Grids of flow domain
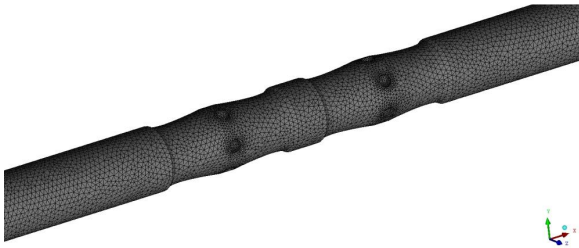
(b) Prism grids near the tube wall

Fig. 3. Schematic of the grid system

3.3.2. Boundaries

In the present work, the fluid is water, and the working temperature is given as 288 K, the corresponding density is 998.2 kg/m^3, viscosity coefficient is 0.001 and Pr is 8.27. The inlet is set as the velocity inlet with values are 0.4 m/s, 0.6 m/s, 0.8 m/s, 1.0 m/s and 1.4 m/s, respectively. The corresponding Reynolds numbers are 7,753, 11,630, 15,506, 19,383 and 27,136, respectively. The outlet is set as a pressure outlet and the pressure value is 0 Pa. The wall boundary conditions are specified with $T_{\text{wall}} = 338$ K, $u_x = u_y = u_z = 0$.

3.3.3. Grid independence validation

To ensure that the simulation results are free of the grid number, four grids system are chosen to repeat debugging in respect of Nu and f. The primary model is employed as an illustration to test the grid independence. The results are shown in Table 2. It is obvious that Nu and f change by 0.4% and 0.3% as the grid number increases from 3,132,955 to 3,168,270, respectively. It means that when the grid number exceeds 3,132,955, the effect of the grid number on simulation results can be neglected. In order to keep a balance between computational efficiency and accuracy, the grid system of 3,132,955 cells is chosen for the grid independence validation.

Table 2
Grid independence validation (Re = 19,383)

Number of cells	Nu	|Nu error (%)|	f	|f error (%)|
3,058,930	137.04	Baseline	0.02676	Baseline
3,100,715	135.41	1.19	0.02654	0.8
3,132,955	134.83	1.6	0.02645	1.2
3,168,270	134.28	2	0.02635	1.5

3.3.4. Validation of numerical method

To validate the accuracy of the numerical method, the simulation results are compared with the empirical correlations in terms of Nu and f. The empirical correlation of Nu_T can be expressed as [9]:

$$Nu_T = \frac{(f_T/8)(Re - 1000) Pr}{1 + 12.7 (f_T/8)^{1/2} \left(Pr^{2/3} - 1 \right)} \left[1 + \left(\frac{D}{L} \right)^{2/3} \right] c_t . \tag{9}$$

The empirical correlation of f_T can be calculated as follows [9]:

$$f_T = (1.82 \lg Re - 1.64)^{-2} . \tag{10}$$

The comparison between the numerical and empirical results as shown in Fig. 4. From Fig. 4, it can be seen that the variation trend of the numerical results is consistent with the empirical correlations. That is, with the increase of Reynolds number,
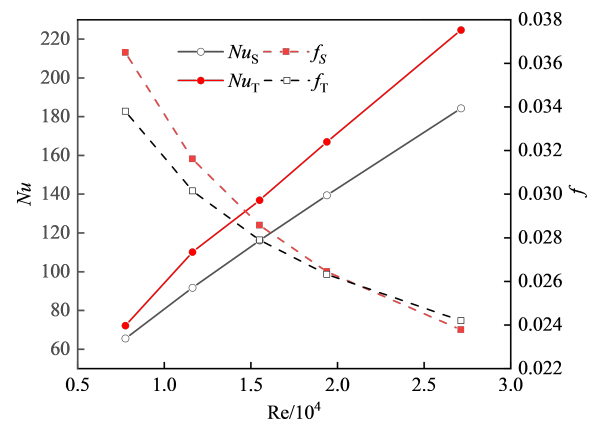

Fig. 4. Comparison of numerical results of Nu and f with empirical correlation

Nusselt number increases, and friction factor decreases. The largest deviations for Nu and f are 18% and 8%, respectively, which are less than 20% (the maximum deviation of 90% of the experimental data from the empirical correlation is within $\pm 20\%$). It means that the numerical results agree well with the empirical correlations. For further validation, Fig. 5 shows the $y+$ distribution along the tube wall, which clearly meets the requirement of $y+ \approx 1$. Therefore, the validation results for the plain tube confirmed the correction of the simulation method used in the present study.
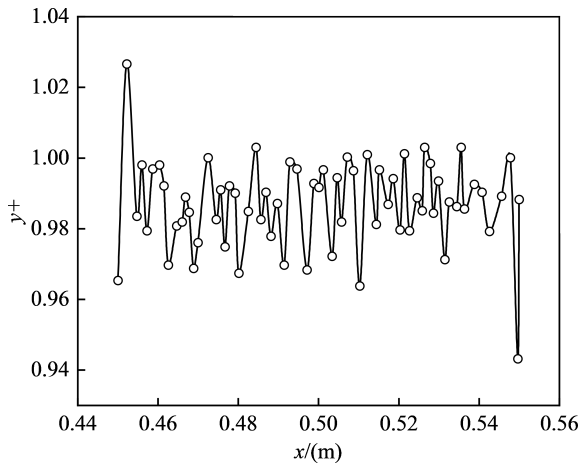

Fig. 5. $y+$ distribution along the tube wall

4. RESULTS AND DISCUSSION

4.1. Flow characteristics

Figure 6 shows the velocity magnitude distribution of $Y = 0$ m plane and for different X planes along the flow direction. As can be seen in Fig. 6a, the velocity profile of the plain tube
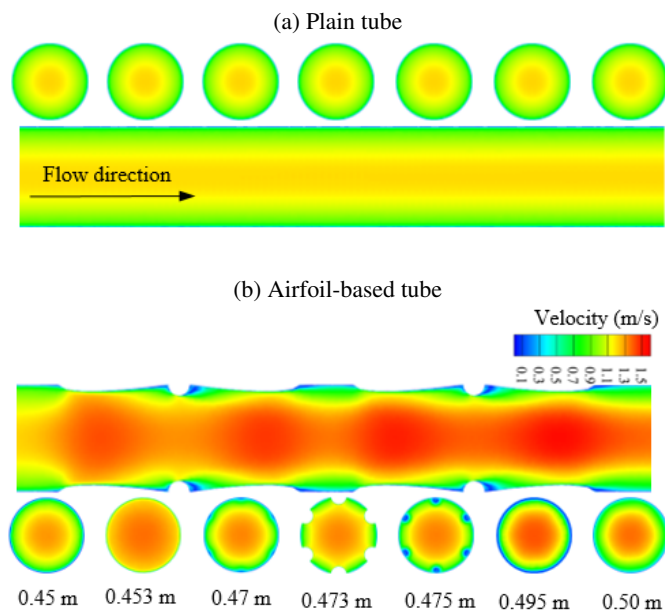

Fig. 6. Velocity magnitude distribution of $Y = 0$ m plane and for different X planes along the flow direction (Re = 19,383, $N = 6$, $\alpha = 0°$, $H/D = 0.1$)

is relatively uniform: the minimum velocity occurs near the tube wall and the maximum velocity occurs at the center of the tube. Contrary to the plain tube, the velocity profile of the airfoil-based tube fluctuates greatly, accompanied by several high-velocity regions and low-velocity regions. Compared with the plain tube, the average velocity and maximum velocity of the airfoil-based tube are greater, which are 1.24 and 1.53 times higher than that of the plain tube, respectively. The local velocity increases along the airfoil or dimples surface, reaching the maximum at about 1/6 of the airfoil and about 1/2 of the surface of the dimples. At this time, the boundary layer separates and vortexes are generated at the forward and backward of the dimples surface. In addition, the flow direction also changes due to the shape change of the tube wall. The above phenomena will enhance the turbulence of the fluid, weaken the thickness of the boundary layer, and thus improve the heat transfer performance, but at the same time, it will increase the flow drags.

4.2. Heat transfer characteristics

Figure 7 shows the local Nu distribution for Re = 19,383 along the flow direction. As shown in Fig. 7, the variations of the local Nu for the plain tube can be ignored, and the average value is 133.46. On the Contrary, the variations of the local Nu are more obvious for the airfoil-based tube, the maximum local Nu is nearly 4.92 times greater than that of the plain tube, and the average Nu is 1.68 times that of the plain tube. Five peaks of Nu appear along the flow direction. Peak 1, Peak 2, Peak 4, and Peak 5 are dominated by the fluid flow impinging onto the upstream surface, which leads to a higher local Nu than that in other regions. Peak 3 appears due to the formation of vortexes, which intensify the flow mixing and thus enhance the local heat transfer performance in this location. In addition, the local Nu gradually increases along the leading edge of the airfoil or dimple, reaching its maximum when the boundary layer separates, at about 1/3 position of the airfoil surface and about 1/2 position of the dimple surface, and then gradually decreases. It is worth noting that between the peaks, the local heat transfer capacity is
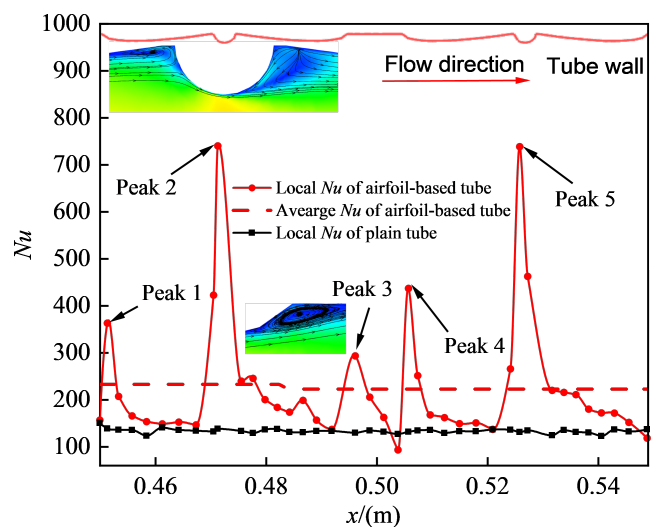

Fig. 7. Local Nu distribution for Re = 19,383 along the flow direction ($N = 6$, $\alpha = 0°$, $H/D = 0.1$)

4

Bull. Pol. Acad. Sci. Tech. Sci., vol. 70, no. 4, p. e141984, 2022

weaker, which is only slightly higher than that of the plain tube. In these regions, the velocity magnitude is relatively small, the flow direction is nearly parallel to the mainstream direction, and the turbulence intensity is weak, so the heat transfer capability is poor.

4.3. Effect of geometric parameters on performance

4.3.1. Effect of the dimples number

Figure 8 shows the effect of the dimples number on the performance of the airfoil-based tube with Re ranging from 7,753 to 27,316. According to Fig. 8a, for the same dimples number, the
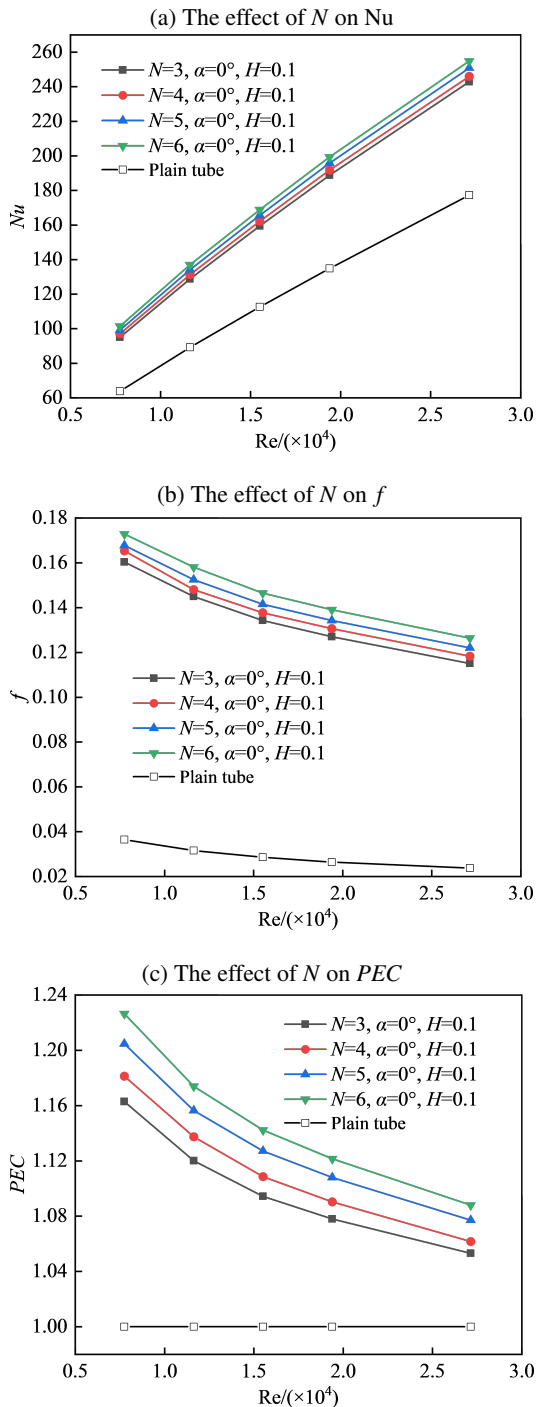
average Nu increases approximately linearly with the increase of Re. For the same Re, the average Nu increases with the increase of the dimples number. When $N = 6$ and Re $= 7,753$, the average Nu obtains its largest value, which is 1.44 times that of the plain tube.

As shown in Fig. 8b, for the same dimples number, the friction factor is inversely related to Re. For the same Re, the friction factor grows with the increase of the dimples number. When $N = 6$ and Re $= 7,753$, the friction factor obtains its largest value, which is 4.8 times that of the plain tube. Two factors may be contributing to this phenomenon. On the one hand, more dimples lead to higher local resistance because it narrows the cross-sectional area of the airfoil-based tube. On the other hand, as mentioned before, vortexes are generated both upstream and downstream of the dimples surface, which also leads to the increase of local resistance.

The above analysis shows that the enhanced airfoil-based tube with dimples has a realizable heat transfer performance with a relatively high-pressure loss penalty. To comprehensively evaluate the effect of the dimples number on the performance of the airfoil-based tube, Fig. 8c presents the variations of PEC with varying Re for different N. The PEC decreases with the increase of Re for different N. When Re is less than 15,506, the PEC decreases sharply with the increase of Re. As Re continues increasing, the curve of PEC variations levels out. In addition, the PEC increases with the increase of N. The maximum PEC value of 1.23 occurs at $N = 6$ and Re $= 7,753$, and the minimum PEC value of 1.05 is obtained by $N = 3$ at Re $= 27,136$.

Further, Fig. 9 presents the temperature and velocity distribution for four different dimples number on the $X = 0.4725$ m plane when $\alpha = 0°$, $H/D = 0.5$ and Re $= 19,383$. Apparently, the average temperature and velocity magnitude grow with the increase of the dimples number. The temperature gradient is much more distinct, and the velocity profile is much more uniform. The cross-sectional area is further reduced with the increase of the dimples number, not only the flow direction is changed but also the velocity magnitude is enhanced, which improves the heat transfer performance of the airfoil-based tube.
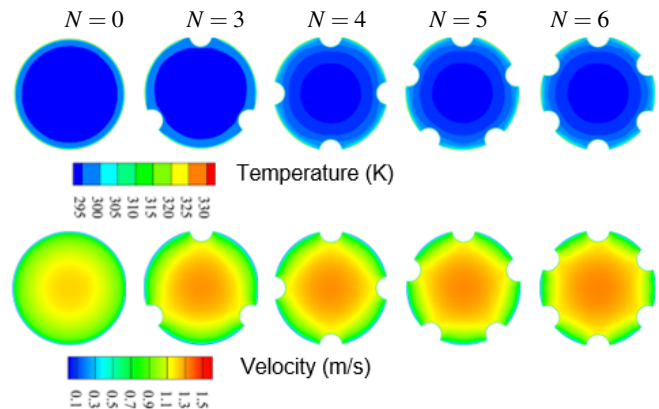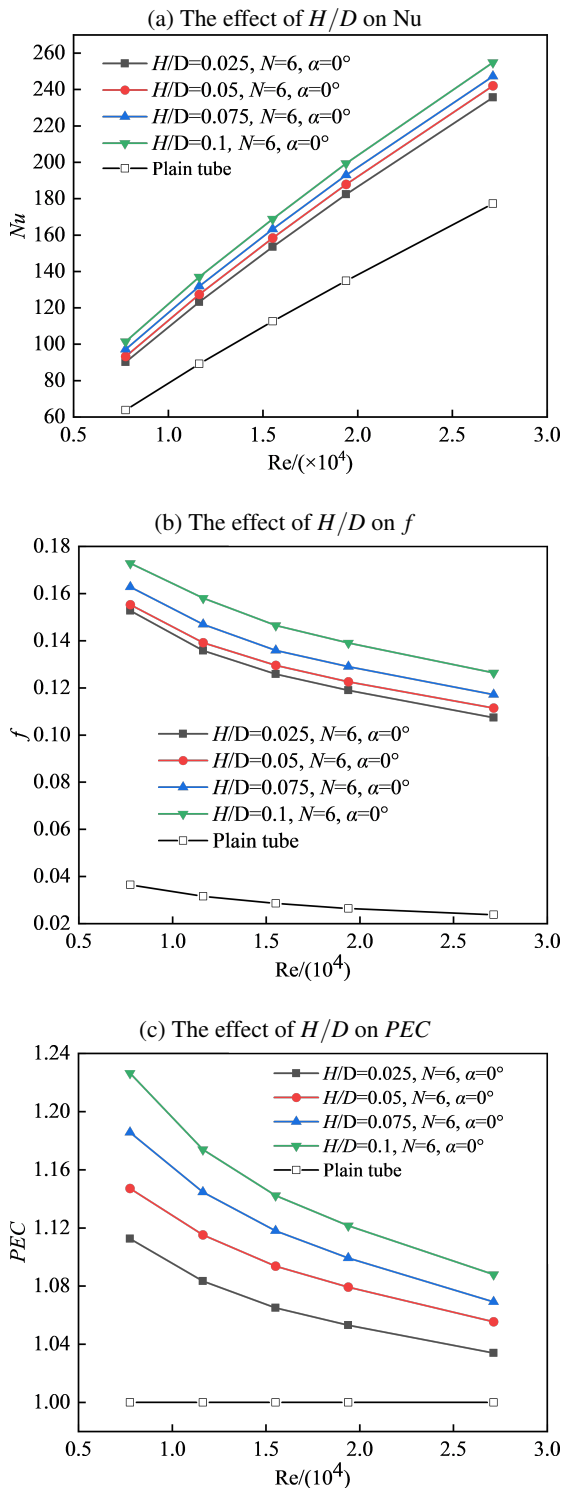

(a) The effect of N on Nu

(b) The effect of N on f

(c) The effect of N on PEC

Fig. 8. The effect of N on the performance of the airfoil-based tube

Fig. 9. The temperature and velocity distribution for four different dimple number on the $X = 0.4725$ m plane ($\alpha = 0°$, $H/D = 0.1$, Re $= 19,383$)

H. Pei, M. Liu, K. Yang, Z. Li, and C. Liu

4.3.2. Effect of the relative depth

Figure 10 shows the effect of the relative depth on the performance of the airfoil-based tube with the Re range from 7,753 to 27,316. It is obvious that the impacts of the relative depth on the performance show the same regularity as that of the dimples number. For the same relative depth, the larger the Re, the larger the Nu, the smaller the f, and the smaller the PEC. For the same Re, with the increment of the relative depth, the Nu, f, and PEC all ascend gradually. The relative depth $H/D = 0.189$ and the Re = 7,753 provide the smallest average Nu, which is 1.49 times that of the plain tube. The airfoil-based tube with $H/D = 0.189$ and Re = 27,136 obtained the smallest PEC value about 1.06 in this case.

Figure 11 presents the local Nu distribution of the tube wall for four different relative depths along the flow direction. Generally, the variations of the local Nu for different relative depths show a similar distribution regularity. The main difference is reflected in the height of Peak 2. The larger the relative depth, the more evident the Peak 2, and the smaller the difference between Peak 2 and Peak 5. In addition, as the relative depth gets larger, the local Nu symmetrically increases on both sides of the dimple, which further accounts for the heat transfer enhancement mechanisms as the relative depth increases.
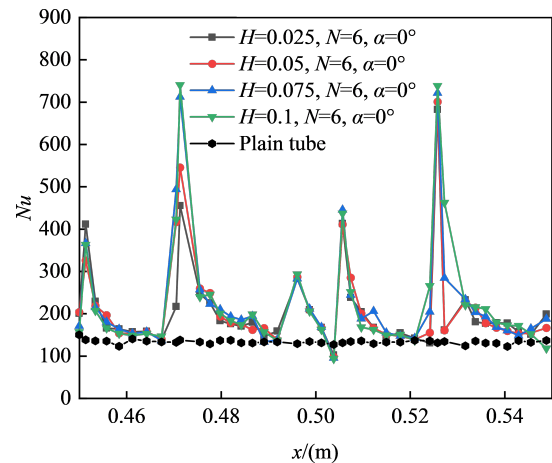
Fig. 11. The local Nu distribution of the tube wall for four different relative depth along the flow direction (Re = 19,383)

Further, Fig. 12 shows the local velocity streamlines in the tube and around the dimples. As can be seen in Fig. 12, for a smaller relative depth, the cross-sectional area is large, and the variation of the velocity magnitude and the flow direction is not appreciable. In such situations, the fluid can flow past the dimples surface smoothly and no vortexes are generated. For a larger relative depth, several vortexes near the dimples could be generated and the velocity magnitude is increased due to the blockage effect. These are the main reasons that result in the increase of Nu with the increase of the relative depth.

4.3.3. The effect of the cross-distribution angle

Figure 13 shows the effect of the cross-distribution angle on the performance of the airfoil-based tube. The data indicates barely noticeable changes in the respect of Nu, f, and PEC for the four dimples number when the Re is constant. For example, the maximum variations of Nu, f, and PEC respectively are only 0.25%, 0.61%, and 0.19% when the cross-distribution angle increases from 0° to 30°. Therefore, it is believed that the effect of the cross-distribution angle on the performance can be ignored and 0° can be applied to the engineering applications as the first choice.

Fig. 10. The effect of H/D on the performance of the airfoil-based tube

6

Bull. Pol. Acad. Sci. Tech. Sci., vol. 70, no. 4, p. e141984, 2022

(a) $H/D = 0.025$

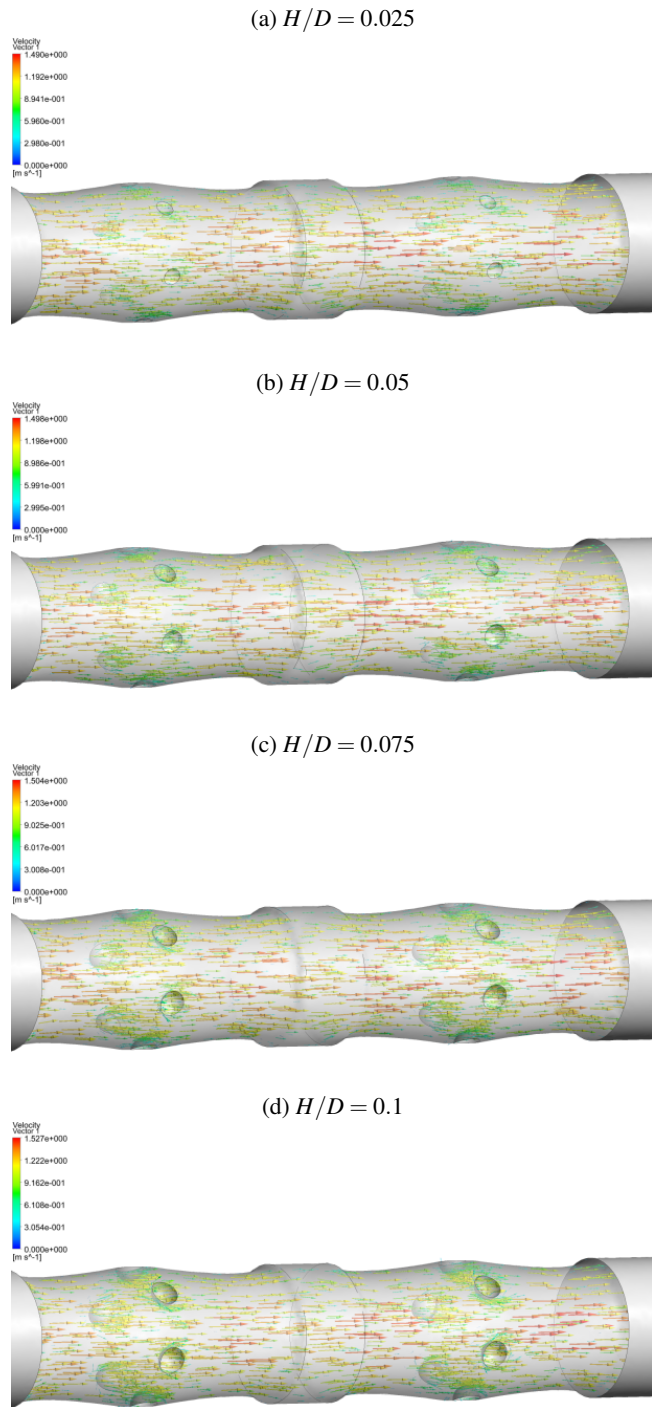(b) $H/D = 0.05$

(c) $H/D = 0.075$

(d) $H/D = 0.1$

Fig. 12. The local velocity streamlines in the tube and around the dimples ($N = 6$, $\alpha = 0°$ Re $= 19,383$)

4.4. Empirical formulas for Nu and f

On the basis of the results from numerical simulation, the empirical formulas for Nu and f are fitted in terms of dimples number N, relative depth H/D, and Reynolds number Re with the errors within $\pm 5\%$, as shown in Figs. 14 and 15:

$$\text{Nu} = 0.1263\text{Re}^{0.7474}N^{0.0676}(H/D)^{0.0629}, \tag{11}$$

$$f = 1.8964\text{Re}^{-0.2598}N^{0.0897}(H/D)^{0.104}. \tag{12}$$

(a) The effect of α on Nu

(b) The effect of α on f

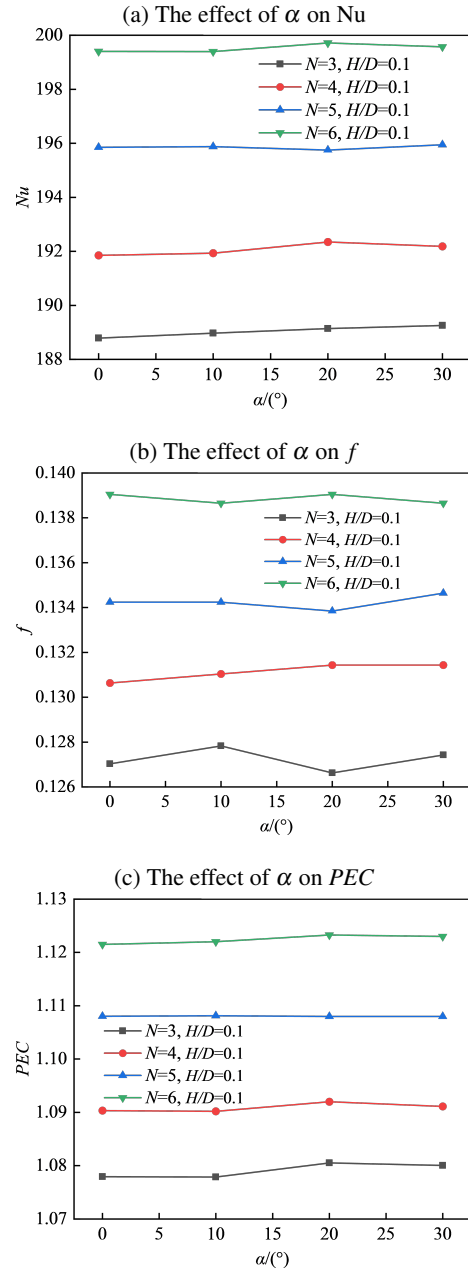(c) The effect of α on PEC

Fig. 13. The effect of cross-distribution angle on the performance of the airfoil-based tube (Re $= 19,383$)
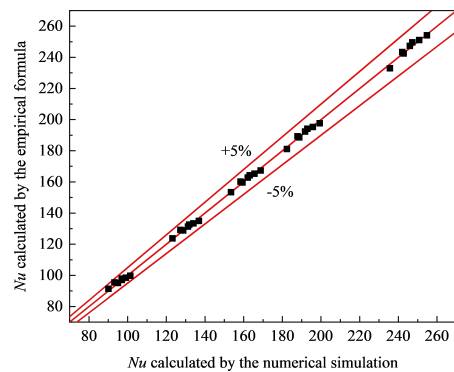
Fig. 14. Deviations of Nu calculated by the empirical formula and numerical simulation

Bull. Pol. Acad. Sci. Tech. Sci., vol. 70, no. 4, p. e141984, 2022

7
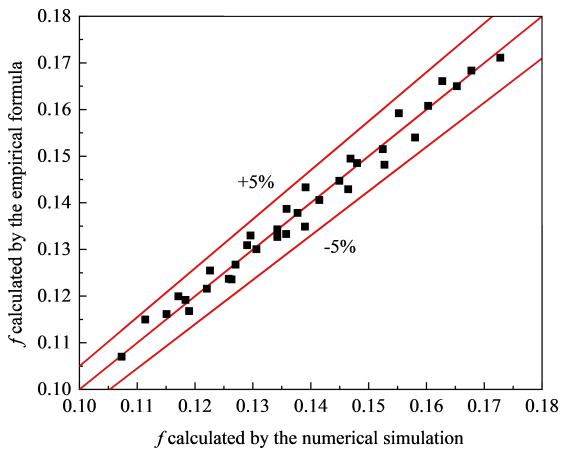
Fig. 15. Deviations of f calculated by the empirical formula and numerical simulation

5. CONCLUSIONS

Three-dimensional flow and heat transfer characteristics of a novel airfoil-based tube with dimples are numerically investigated in the present work. The velocity contour, temperature contour, and local streamlines are presented to illustrate the heat transfer enhancement mechanisms. The effect of the dimples number, relative depth, cross-distribution angle, and Reynolds number on the performance is also analyzed. The results are summarized as follows:

- In contrast to the plain tube, not only is the velocity magnitude changed but also the flow direction is altered. Vortexes are also generated around the dimples for large relative depth situations. All these changes can improve the flow mixing and interrupt the boundary layer, thus enhancing the heat transfer performance of the airfoil-based tube, meanwhile, resulting in a relatively high-pressure loss penalty. In the range of design parameters considered, the maximum increase of the average Nu is up to 68%, meanwhile, the friction factor is 3.74 times than that of the plain tube.

- Several peaks of Nu occur along the flow direction. The height of Peak 2 is strongly correlated to the relative depth. The local Nu obtains the largest value when $Re = 19{,}383$, $N = 6$, $\alpha = 0°$, $H/D = 0.1$, which is increased by 392% as compared to that of the plain tube.

- The performance of the airfoil-based tube is significantly affected by the Reynolds number, dimples number, and relative depth, but the effect of the cross-distribution angle can be neglected. The more the dimples number, the larger the relative depth, and the smaller the Reynolds number, the better the comprehensive performance. In the present study, the *PEC* of the airfoil-based tube reaches the maximum value about 1.23 when $N = 6$, $H/D = 0.1$, $\alpha = 0°$ and $Re = 7{,}753$.

REFERENCES

[1] M. Kmiotek and A. Kucaba-Pital, "Influence of slim obstacle geometry on the flow and heat transfer in microchannels," *Bull. Pol. Acad. Sci. Tech. Sci.*, vol. 66, no. 2, pp. 111–118, 2018, doi: 10.24425/119064.

[2] M. Ge, "Numerical investigation of flow characteristics over dimpled surface," *Therm. Sci.*, vol. 20, no. 3, pp. 903–906, 2016.

[3] R. Maithani and A. Kumar, "Correlations development for Nusselt number and friction factor in a dimpled surface heat exchanger tube," *Exp. Heat Transfer*, vol. 33, no. 2, pp. 1–22, 2019, doi: 10.1080/08916152.2019.1573863.

[4] R. Vinze, A. Khade, P. Kuntikana, and M. Ravitej, "Effect of dimple pitch and depth on jet impingement heat transfer over dimpled surface impinged by multiple jets," *Int. J. Therm. Sci.*, vol. 145, no. 2, p. 105974, 2019, doi: 10.1016/j.ijthermalsci.2019.105974.

[5] N.A. Kiselev, A.I. Leontiev, Y.A. Vinogradov, and A. Zditovets, "Effect of large-scale vortex induced by a cylinder on the drag and heat transfer coefficients of smooth and dimpled surfaces," *Int. J. Therm. Sci.*, vol. 136, pp. 396-409, 2019, doi: 10.1016/j.ijthermalsci.2018.11.005.

[6] Z. Liang, S. Xie, L. Zhang, J. Zhang, Y. Wang, and Y. Yin, "Influence of geometric parameters on the thermal hydraulic performance of an ellipsoidal protruded enhanced tube," *Numer. Heat Transfer Part A, Appl.*, vol. 72, no. 2, pp. 153–170, 2017, doi: 10.1080/10407782.2017.135900.

[7] L. Zheng, D. Zhang, Y. Xie, and G. Xie, "Thermal performance of dimpled/protruded circular and annular micro-channel tube heat sink," *J. Taiwan Inst. Chem. Eng.*, vol. 60, pp. 342–351, 2016, doi: 10.1016/j.jtice.2015.10.026.

[8] L. Zhang, W. Xiong, J. Zheng, Z. Liang, and S. Xie, "Numerical analysis of heat transfer enhancement and flow characteristics inside cross-combined ellipsoidal dimple tubes," *Case Stud. Therm. Eng.*, vol. 25, p. 100937, 2021, doi: 10.1016/j.csite.2021.100937.

[9] Y. Wang, Y. He, Y. Lei, and R. Li, "Heat transfer and friction characteristics for turbulent flow of dimpled tubes," *Chem. Eng. Technol.*, vol. 32, no. 6, pp. 956963, 2009, doi: 10.1002/ceat.200800660.

[10] W. Liao, X. Liu, and H. Zhang, "Influence of number of elliptical dimples and their distribution on flow and heat transfer performance of tube," *J. Pressure Vessel Technol.*, vol. 37, no. 4, pp. 38–45,67, 2020, doi: 10.3969/j.issn.1001-4837.2020.04.006.

[11] K. Zhang, F. Wang, and Y. He, "Numerical study on flow and heat transfer performance of a new type of biomimetic tube," *J. Eng. Thermophys.*, vol. 40, no. 2, pp. 375–381, 2019.

[12] S. Xie, Z. Liang, L. Zhang, and Y. Wang, "A numerical study on heat transfer enhancement and flow structure in enhanced tube with cross ellipsoidal dimples," *Int. J. Heat Mass Transfer*, vol. 125, pp. 434–444, 2018, doi: 10.1016/j.ijheatmasstransfer.2018.04.106.

[13] H. Shi, H. Liu, J. Xiong, Y. Qiu, and Y. He, "Study on flow and heat transfer characteristics of an airfoil printed circuit heat exchanger with dimples," *J. Eng. Thermophys.*, vol. 40, no. 4, pp. 857–862, 2019.

[14] R. Li, Y. He, P. Chu, and Y. Lei, "Numerical simulation of dimpled tube for heat transfer enhancement," *J. Eng. Thermophys.*, vol. 29, no. 11, pp. 1947–1949, 2008, doi: 10.3321/j.issn:0253-231X.2008.11.038.

8

Bull. Pol. Acad. Sci. Tech. Sci., vol. 70, no. 4, e141984, 2022

[15] F. Chen, L. Zhang, X. Huai, J. Li, H. Zhang, and Z. Liu, "Comprehensive performance comparison of airfoil fin PCHEs with NACA 00XX series airfoil," *Nucl. Eng. Des.*, vol. 325, pp. 42–50, 2017, doi: 10.1016/j.nucengdes.2017.02.014.

[16] S. Xie, Z. Liang, L. Zhang, and Y. Wang, "Numerical investigation on heat transfer performance and flow characteristics in enhanced tube with dimples and protrusions," *Int. J. Heat Mass Transfer*, vol. 122, no. JUL, pp. 602–613, 2018, doi: 10.1016/j.ijheatmasstransfer.2018.01.106.

[17] X. Zhang, Z. Liu, and W. Liu, "Numerical studies on heat transfer and flow characteristics for laminar flow in a tube with multiple regularly spaced twisted tapes," *J. Eng. Thermophys.*, vol. 58, no. 2, pp. 157–167, 2012, doi: 10.1016/j.ijthermalsci.2012.02.025.

[18] Z. Cao, Z. Wu, H. Luan, and B. Sunden, "Numerical study on heat transfer enhancement for laminar flow in a tube with mesh conical frustum inserts," *Numer. Heat Transfer Part A, Appl.*, vol. 72, no. 1, pp. 21–39, 2017, doi: 10.1080/10407782.2017.1353386.

[19] H. Usui, Y. Sano, K. Iwashita, and A. Isozaki, "Enhancement Effect for Heat Transfer by Combined Use of Internally Grooved Rough Surfaces and Twisted Tapes," *Kagaku Kogaku Ronbunshu*, vol. 10, no. 3, pp. 280–286, 1984, doi: 10.1252/kakoronbunshu.10.280.

[20] V. Gneilinski, "New equations for heat and mass-transfer in turbulent pipe and channel flow," *Int. Chem. Eng.*, vol. 16, pp. 359–368, 1976.

Bull. Pol. Acad. Sci. Tech. Sci., vol. 70, no. 4, p. e141984, 2022

9